NONLINEAR PROBLEMS OF CAVITATION BREAKDOWN OF LIQUIDS UNDER EXPLOSIVE LOADING (REVIEW)

V. K. Kedrinskii

UDC 532.593+532.529+541.126

The breakdown of a liquid in intense rarefaction waves produced by explosive loading near the free surface represents a new field in the hydrodynamics of explosions. Only a few of the relevant concepts, such as critical tensile stress and tensile strength in liquids, have a long history. The first studies were static in nature and the first results in this field were published in the middle of the last century by Berthelot [1]. The first dynamical study using an underwater explosion near a free surface was evidently that of Hilliar in 1919 [1]. In a recent study by Wilson et el. [2] the strength of a liquid was estimated by measuring the velocity of the spray dome produced by shallow underwater explosions. The critical tensile stress p_* was determined by the amplitude of the wave p at which the velocity of the free surface $v = (2p - p_*)/\rho U$ became equal to zero. The resulting value of p_* was 0.85 MPa for standing tapwater and 1.5 MPa for deionized and vacuum-evaporated water. Carlson and Henry [3] used high-speed loading of a thin liquid layer by a pulse electron beam and obtained the value $p_* = 60$ MPa.

Practically all of the experiments rely on visible discontinuities in the liquid, which by nature are determined by strongly nonlinear cavitation developing on cavitation nuclei in the presence of intense rarefaction waves. These discontinuities (sheets) were observed by the author in experiments using underwater explosions of line charges (two-dimensional problem) near the free surface [4]. It was noted that sheet discontinuities form only in a narrow layer near the free surface, in spite of the fact that strong cavitation extends over a volume an order of magnitude larger. The sheets themselves are strongly cavitating layers and their structure recalls foam, which then rapidly breaks up into separate drops, forming the spray dome [5]. Because of the strong cavitation the two-phase state of real liquids must be taken in mathematical models for the wave field [6].

The breakdown of a liquid under explosive loading comprises a series of essentially nonlinear phenomena. It can be defined as the inversion of the two-phase state of the medium, i.e., the transformation of the cavitating liquid into a gas-droplet system. The inversion comprises the following stages:

a) the formation and dynamics of bubble clusters;

b) unbounded multiplication of cavitation nuclei leading to a foamy structure;

c) breakup of the foamy structure into cavitating fragments;

d) transition into the droplet state and its evolution.

Each of these stages is self-contained and yet forms an integral part of the process. Therefore the mechanisms corresponding to each stage are of great interest.

In the present review paper we consider the basic results for each stage, including the experimental data, the experimental methods, and the physical and mathematial models of the processes.

1. Bubble Cavitation. In physical acoustics this stage has been studied the most. The main problems are to determine the state of a real liquid from the point of view of its homogeneity and the mechanism of bubble cluster formation. The construction of a mathematical model to describe cavitating liquids is obviously important since it could then be used to analyze the structure and the parameters of the wave field and the limiting values of the tensile stress allowed by a cavitating liquid.

Novosibirsk. Translated from Prikladnaya Mekhanika i Tekhnicheskaya Fizika, No. 3, pp. 74-91, May-June, 1993. Original article submitted June 29, 1992.

0021-8944/93/3403-0361$12.50

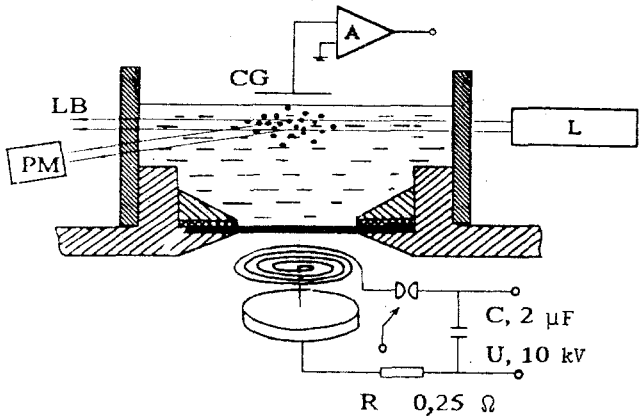

Fig. 1

In contrast to the process of fracture in solids, in the case of pulse loading in liquids there is no stage in which fracture centers develop. The macroscopic structure of the liquid is such that even when the liquid is carefully purified by distillation and deionization there are always microinhomogeneities present which can act as cavitation nuclei. They can be microbubbles of free gas, solid particles, or their conglomerates. The determination of the nature of these microinhomogeneities, their density, and their size spectrum, is one of the basic problems in the study of the state of a real liquid.

The most reliable results in this field are obtained by a combination of light scattering and shock tubes. A typical experimental setup is shown schematically in Fig. 1. It represents an electromagnetic source of a pulse magnetic field generated in a narrow gap between a membrane and a plane helical coil on which a high-voltage capacitor is discharged [7]. The parameters of the discharging circuit are chosen to ensure that the discharge is aperiodic and to thereby eliminate pressure oscillations in the shock wave created in the liquid by the motion of the membrane driven by the magnetic field. This method can generate shock waves with amplitudes up to 10 MPa and durations of the positive phase of about 3 msec. The liquid is placed in the working (transparent) section of the shock tube. The light source is an He–Ne laser L whose beam LB of diameter 1.5 mm is transmitted at a depth of 3 mm from the free surface of the liquid. The scattered light is collected by a photomultiplier system PM whose position relative to the direction of the laser beam is chosen taking into account the specific features of the problem. The signal from the photomultiplier is fed into a digital-analog transducer and a computer. The capacitor pickup CG through the amplifier A measures the displacement of the free surface resulting from reflection of the shock wave.

The angular distribution of the scattered intensity (the so-called scattering indicatrix) has characteristics which are a record of the sizes of the microinhomogeneities. Smoothed maxima indicate size dispersion of the nuclei. In the case of microbubbles of free gas the light must be specially polarized. Static experiments (unperturbed liquid) with distilled water and a wavelength of $\lambda = 0.63$ μm of the scattered light show that the radii of the nuclei are approximately 1.5 ± 0.2 μm and are nearly monodispersed [7]. We note that this result is associated with a certain selectivity of the detection system which limits its capability of determining the true distribution. The distribution and sizes of microparticles in distilled water were studied by the author together with V. A. Stepanov using the Malvern Instrument M6.10. Of the data obtained the maximum of the distribution was considered to be relatively reliable: in fresh water it was about 4 μm and in standing water it was 0.85 μm (with a magnetic mixer). The experimental results of [8] in standing water were fit in [9] to the simple relation $N_i^{\frac{2}{3}}V_i \approx C = \text{const}$, where i is the bubble species, N_i is the number of bubbles of a given species, V_i is their volume, and $C = 10^{-9}$. Obviously this relation does not describe the entire distribution, which from physical considerations should have a maximum and asymptotically approach zero as the volume of bubbles approaches zero and infinity. A distribution with these properties is

$$N_i = N_0 \frac{(V_i/V_*)^2}{1 + (V_i/V_*)^4}. \qquad (1.1)$$

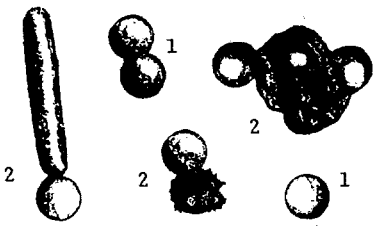

Fig. 2

TABLE 1

Author	R_0, μm	N_0, cm^{-3}	k_0
Strasberg (1956)	6 22 13	$\leqslant 1$ $\ll 1$ $\ll 1$	$6 \cdot 10^{-10}$ $2 \cdot 10^{-10}$ $3 \cdot 10^{-10}$
Gavrilov (1970)	50—0,5 *	$\leqslant 1$	10^{-8}—10^{-12}
Hammitt (1974)	6 3	$\simeq 1$ $\simeq 100$	
Besov et al. (1984)	1,5	10^3—10^4 (10^5—10^6)	$<10^{-6}$

*The range of sizes of nuclei observed during the settling of a sample of fresh tap water over a period of several hours.

This distribution involves two unknown parameters: the total number of bubbles per unit volume N_0 and the normalization parameter V_*, which can be taken as the volume of a bubble of radius R_* corresponding to the maximum of the distribution. As shown above $R_* \simeq 0.85$ μm. Then since the tail of the distribution (1.1) must fit the data of [8] for $R_i \geq 3$ μm, the total density of microinhomogeneities is then $N_0 = 1.5 \cdot 10^5$, which is consistent with the estimate 10^5-10^6 cm^{-3} [10] obtained by measuring the tracks of diffraction spots from light scattered by microinhomogeneities.

Study of the dynamics of the scattering indicatrix as the shock wave passes through the sample of distilled water shows that its intensity can vary above or below the background for two special detection angles, assuming that microparticles can deform under the influence of the shock wave [7]. Experimental support of this fact is direct proof of the existence of microbubbles of free gas among cavitation nuclei.

Two problems associated with the state of a real liquid are the stabilization of nuclei and their density N per unit volume, which directly affects the mechanism of bubble cluster formation in rarefaction waves. Several models have been proposed to solve the first problem:

a) fluctuating vacancies: $R_* = (kT/\sigma)^{1/2}$ (Frenkel, 1945);

b) hydrophobic particles with nuclei in the interstices $R_* = 2\sigma/p_0$ (Harvey, 1944);

c) surface organic films (Herzfeld and Fox, 1954);

d) ionic mechanism (Blake, 1949, and Akulichev, 1966);

e) solid-particle nuclei (Plesset, 1969);

f) microbubbles with heat fluxes, Stokes forces, and buoyancy forces in equilibrium: $R_* = (\nu^2 kT/\rho_0 g^2)^{1/7}$ (Kedrinskii, 1985);

g) combination structures (experimental results, Fig. 2) (Besov, Kedrinskii, and Pal'chikov, 1991).

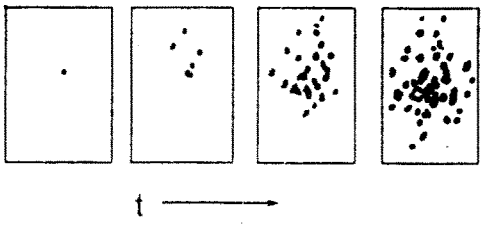

Fig. 3

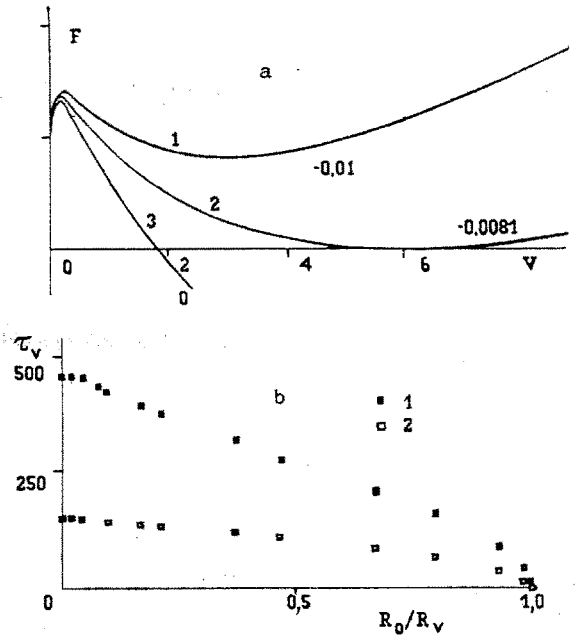

Fig. 4

All of the above types of microinhomogeneities with their stabilization properties can exist in a real liquid and hence there is a wide distribution of sizes from nanometers to tens of microns. The second problem is to determine the number of nuclei N_0 in the cavitation zone and their volume concentration k_0. Experimental data on these parameters are given in Table 1.

The first three results for the density N_0 include only gas nuclei 1 (Fig. 2), the last result takes into account all types of microinhomogeneities (data in parentheses), including solid nuclei and their combinations 2 with gas nuclei, on which vapor bubbles can grow under tensile stress.

The results of acoustic diagnostics of microbubbles of free gas (obtained in particular by Strasberg) indicate a very low density. However, high densities are observed in fully developed cavitation clusters. This suggests an avalanche-like population of the zone of strong bubble cavitation by nuclei. For example, this model was used in [11] to explain the observed (by high-speed motion pictures) growth of cavitation in the focal zone of an ultrasonic concentrator (f = 550 kHz).

Several frames are shown in Fig. 3 (the interval between frames was three periods and the vertical size was 6 mm). We see that initially after application of the field only a single bubble appears in the frame. Strasberg's results appear to be supported, but after 10 periods cavitation bubbles form a dense cloud near the focus. One assumes that there was an avalanche-like multiplication of nuclei caused by the instability of the shape of the bubbles. Under strong compression the bubbles break up into separate fragments, which then act as new cavitation nuclei. Their future behavior in the ultrasonic field is then assumed to follow that of their "parents." The result is a curious ultrasonic pumping of the liquid by nuclei. Two facts which have not been taken into account in this discussion are:

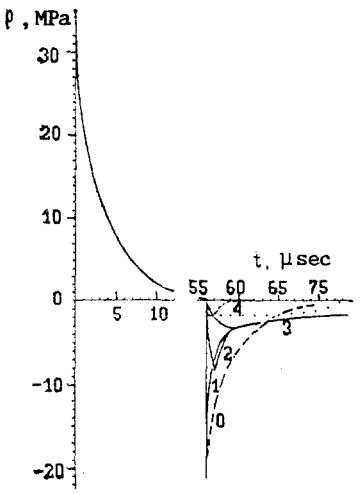

Fig. 5

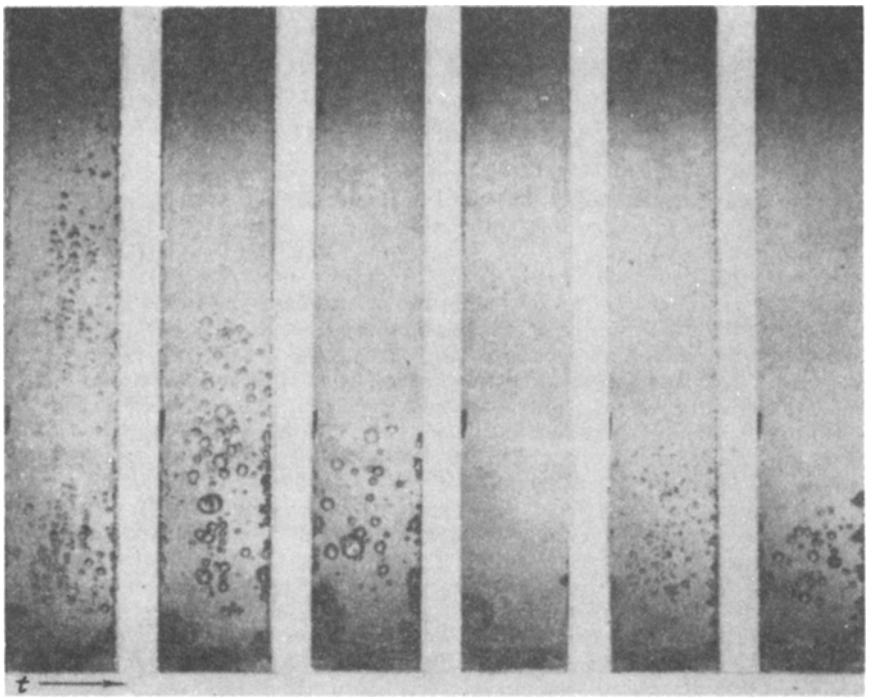

Fig. 6

1) the velocity of the fragments must be so high that they can quickly establish a sufficiently uniform distribution in space;

2) the generation of a dense cavitation zone in the field of a single rarefaction pulse (for example in the case of a shock wave produced by an underwater explosion reflecting from the free surface) is impossible according to the above discussion.

A fundamentally new mechanism for the generation of cavitation zones was proposed by the present author in [12]. The essence of this mechanism is as follows:

a) it is assumed that a real liquid contains a spectrum of nuclei of radii 10^{-7}-10^{-3} cm and constant density of 10^{5}-10^{6} cm^{-3};

b) the concept of visible (detectable) size of a cavitation bubble is introduced;

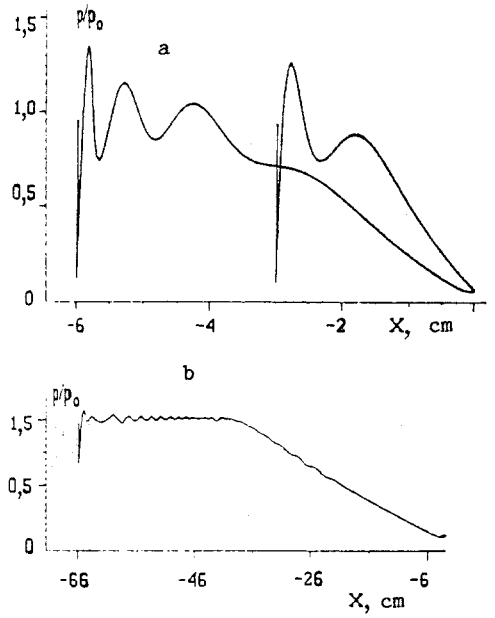

Fig. 7

c) the apparent multiplication of cavitation nuclei in relatively weak ultrasonic fields is explained by the successive saturation of the zone by bubbles attaining visible size after different times, which depend on their initial position in the spectrum of nuclei;

d) for strong rarefaction the entire spectrum of nuclei can reach visible size simultaneously and then the saturation density of the cavitation zone by bubbles reaches a maximum at once.

The last two assertions were based on the theoretical and numerical analysis of the effects of initial size on the time required for a nucleus to grow to a given size [13]. We consider the simplest case of constant tensile stress. The dynamical behavior of a bubble of volume V is determined by the first integral of the Rayleigh equation

$$V^{-1/3}\dot{V}^2 = 6\eta F(V, V_0, p), \tag{1.2}$$

where $F = \frac{1+\mathrm{We}\,V_0^{-1/3}}{\gamma-1} V_0^{\gamma}\left(V_0^{1-\gamma} - V^{1-\gamma}\right) - p(V-V_0) - \frac{3}{2}\,\mathrm{We}\left(V^{2/3} - V_0^{2/3}\right)$; dimensionless variables and parameters were introduced as follows: $V = (R/R_V)^3$; R_V is the visible bubble radius; R_0 is the radius of the nucleus; $V_0 = (R_0/R_V)^3$, $p = p_\infty/p_0$; p_∞ is the pressure at infinity; $\mathrm{We} = 2\sigma/p_0R_V$; $\eta = p_0/\rho_0c_0^2$; a dot denotes a derivative with respect to $t = t'c_0/R_V$. The function F on the right-hand side of (1.2) describes a family of curves dependent upon V_0 and p. A solution exists only for those parts of the curves where $F \geq 0$.

Qualitative analysis shows that for different values of p three types of solution are possible. They are shown in Fig. 4a for $R_V = 0.01$ cm, We = 0.015, $\gamma = 1.4$, and $V_0 = 0.01$. For $p = -0.01$ we have $F > 0$ (curve 1), which implies unbounded growth of the bubble. The asymptotic limit at infinite time is determined by the conditions that both F and its derivative F_V vanish. For the values of the parameters taken above, this corresponds to $p = -0.0081$ and $V = 6$ (curve 2). The third type of solution is a periodic oscillation: the possible values of V are between the points $F = 0$ (curve 3 is obtained for $p = 0$). We note that in this case the bubble is within the visible zone during part of its oscillation period.

Integration of (1.2) from V_0 to 1 determined the time τ_V required for the bubbles to reach visible size. Figure 4b shows τ_V as a function of R_0/R_V for $p = -1$ and -10 (sets of points 1 and 2, respectively) beginning at about 10 μm (the visible size was assumed to be 100 μm). The quantity τ_V is practically constant for smaller sizes. When $R_0 \ll R_V$ the quantity τ_V is described by the simple equation

$$\tau_V \approx 3/\sqrt{6\eta|p|}.$$

Fig. 8

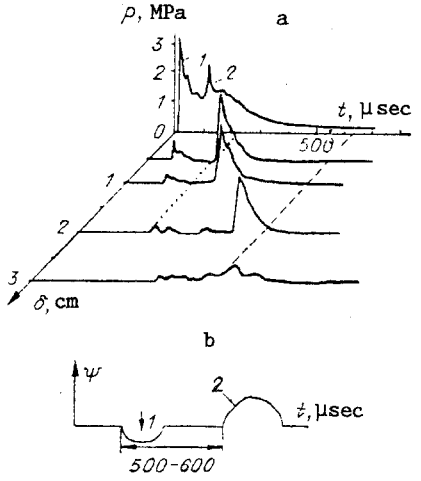

Fig. 9

For the set of points 1 we see that nuclei with $10 < R_0 < 100$ μm reach visible size gradually and the entire spectrum becomes visible about 12 μsec after application of the stress. The calculations show that for $p = -0.01$ bubbles with radii smaller than 17 μm do not reach visible size.

The data support the interpretation of a real liquid as a two-phase medium, in spite of the negligibly small initial gas content (volume concentrations of 10^{-8}-10^{-12} cm^{-3}). It is then logical to assume that the transformation of rarefaction waves in a cavitating liquid is similar to the effect of propagation of shock waves in a bubbly medium and that the mathematical model of such a medium can be used to describe cavitation effects [6]. This model is a system of conservation laws for the average density ρ, the pressure p, and mass velocity v. The state of the medium is described by the dynamical Rayleigh equation for an individual bubble, and the relation between ρ and the volume concentration of the vapor-gas phase k:

$$\begin{gathered} d\rho/dt + \rho \operatorname{div} \mathbf{v} = 0, \quad d\mathbf{v}/dt + \rho^{-1}\nabla p = 0, \\ \rho = (1-k)\rho_l, \quad k = k_0(R/R_0)^3, \\ Rd^2R/dt^2 + (3/2)(dR/dt)^2 = [p_0(R_0/R)^{3\gamma} - p]/\rho_l. \end{gathered} \tag{1.3}$$

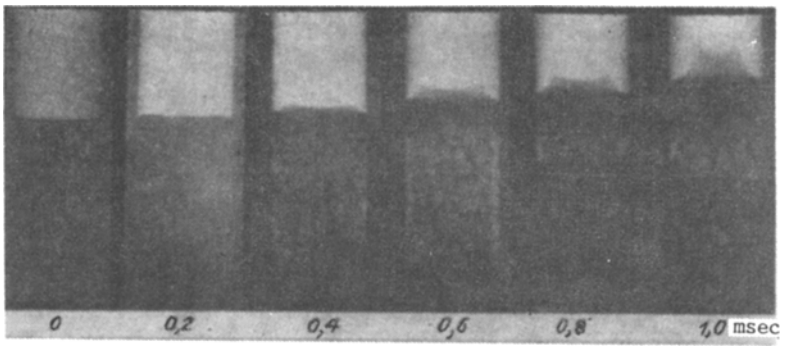

Fig. 10

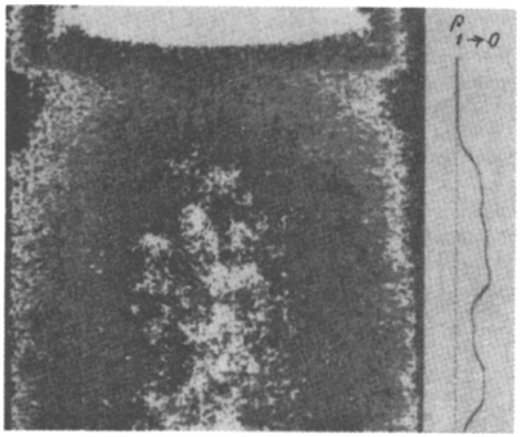

Fig. 11

This model can be used to solve a number of fundamental problems, the most important of which is to predict the limiting tensile stress that can be measured in the liquid. These results were analyzed in [6, 14] using a simplified version of (1.3), based on certain approximations. Since the compressibility of the medium as a whole is determined by the compressibility of the vapor-gas phase, we can assume that the liquid component of the medium (the solvent phase) is incompressible. Nonlinear processes in cavitating liquids are assumed to be a consequence mainly of the nonlinear dynamics of the bubbles. Then the system (1.3) can be reduced to the form

$$\Delta p = -\rho_0 k_0 \partial^2 k/\partial t^2,$$
$$\partial^2 k/\partial t^2 = \left(3/\rho_0 R_0^2\right) k^{1/3} \left(p_0 k^{-\nu} - p\right) + (\partial k/\partial t)^2/6k. \tag{1.4}$$

We next introduce a new spatial variable $\eta = \alpha r k^{1/6}$, where $\alpha = \sqrt{3k_0}/R_0$ and the following two fundamental assumptions:

a) the dynamics of bubbles in a cluster can be described by the equation $k_{tt} \simeq -3k^{1/3}p/\rho_0 R_0^2$, which can then be substituted into the right-hand side of the first equation of (1.4);

b) $|p_{\eta\eta}\eta_r^2| \gg |p_\eta \eta_{rr}|$ and $k \gg |rk_r/6|$, which implies that the pressure in the cavitating liquid obeys an equation of the Helmoltz type

$$\Delta p \simeq p, \tag{1.5}$$

and therefore an analytical relation can be found between the pressure and the concentration of the vapor-gas phase in the cavitating liquid. Simultaneous solution of (1.5) and the Rayleigh equation in (1.3) determines the parameters of the rarefaction wave and the dynamics

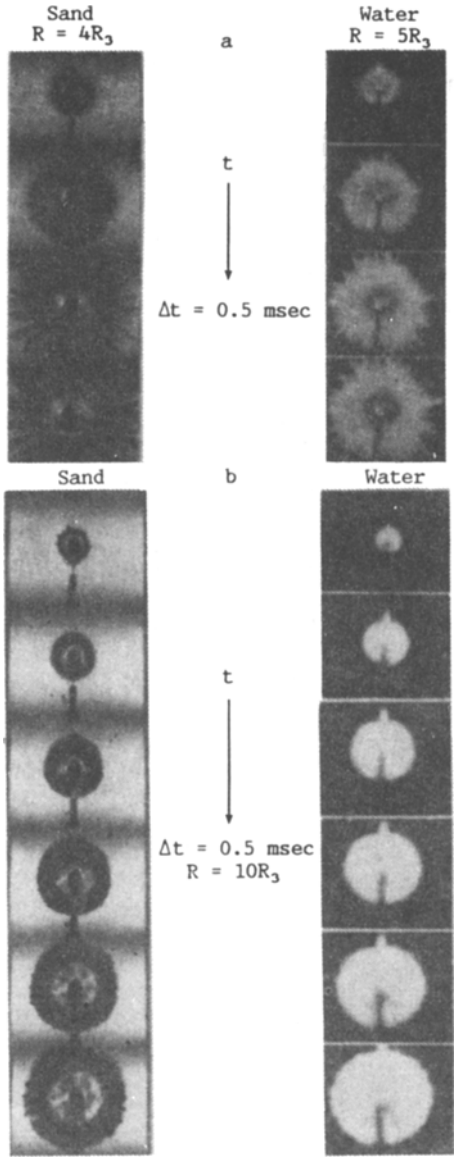

Fig. 12

of the cavitation process [4]. By comparing with the numerical solutions of the complete equations and with experimental data it can be shown that this approximation gives reliable results for the main characteristics of wave process in cavitating liquids.

It is known that the stress at the front of a rarefaction wave is continuous and reaches its maximum value after a finite time Δt^*, which can be defined as the slope of the front. Solution of the axisymmetric problem for the growth of the cavitation zone in an underwater explosion near the free surface shows that this fact is essential in determining the limiting stress [6]. After the time Δt^* the volume concentration k of the vapor-gas phase increases by several orders of magnitude, significantly changing the state of the medium and the applied stress field. As a result, the maximum negative pressure amplitude in a cavitating liquid can be up to an order of magnitude lower [6] than that of an ideal one-phase model.

Figure 5 shows the numerical and experimental data (points) of the rarefaction wave profile at a depth of 4.5 cm near the symmetry axis for an explosion of a 1.2 g charge at a depth of 18.5 cm. Curve 0 represents the one-phase model, curves 1-3 were obtained for R_0 = 5 μm, $k_0 = 10^{-11}$, and Δt^* = 0, 1, and 5 μsec, respectively, and curve 4 corresponds to

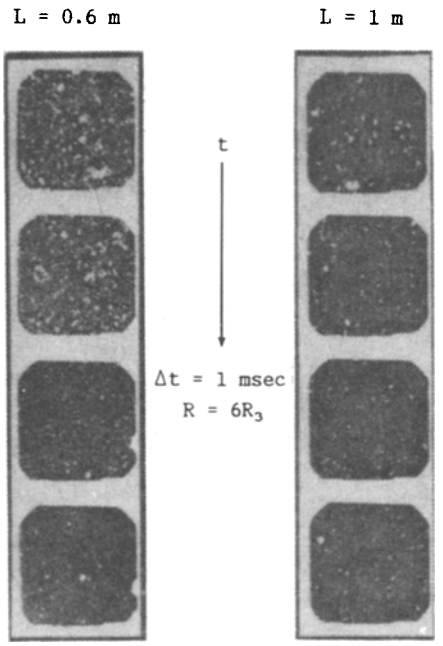

Fig. 13

$k_0 = 10^{-10}$, $\Delta t^* = 1$ μsec. Curves 2 and 4 are distinguished by the volume concentration. Note that the experimental points lie near curve 3 and support the possibility of calculating the real parameters of the wave field.

The tensile stress relaxation time in a cavitating liquid can be estimated both numerically and experimentally for the example of cavitation produced at the bottom of a vertical tube containing the liquid when the tube is suddenly accelerated downward [14]. As shown by the experimental data (Fig. 6) obtained by the author together with I. Hansson and K. Morch at the Danish Technical University, a zone of strong bubble cavitation develops at the bottom of the tube. For sufficiently high acceleration amplitude this cavitation zone can fuse into a continuous vapor-gas layer which will determine the conditions for the detachment of the liquid column from the bottom. The experiment was modeled numerically using the one-dimensional form of (1.5) and the closing equations of (1.3) for the following boundary condition at the bottom of the tube ($z = 0$): $\partial p/\partial z = -\rho_0 a(t)$. Here $a(t)$ is the acceleration of the tube and z is the vertical coordinate. It was assumed for simplicity that the liquid occupies the entire half space $z \geq 0$. The solution of (1.5) gives an analytical expression for $p(k)$:

$$p = -\rho_0 |a(t)| \exp(-\alpha k^{1/6} z)/\alpha k^{1/6}. \tag{1.6}$$

We substitute (1.6) into the Rayleigh equation, which for the dimensionless radius $y = R/R_0$ takes the following form at $z = 0$:

$$y\ddot{y} + (3/2)\dot{y}^2 = (p_0/\rho_0 R_0^2)[y^{-3\nu} + \rho_0 |a(t)|/\alpha y^{1/2} p_0]. \tag{1.7}$$

Neglecting the gas pressure inside the bubbles and considering only their expansion phase, which is justified for the purpose of estimating the relaxation time, the above equation can be solved analytically, given the explicit dependence $a(t)$.

We consider the transformation of a pulse discharge for the model of an underwater shock wave, putting $a(t) = a_{max}\exp(-t/\tau)$, which corresponds to a jump at the front of the rarefaction wave. The value of a_{max} corresponding to $p_{max} = -30$ MPa calculated from (1.6) is $5 \cdot 10^7$ cm/sec^2. The solution of (1.7) has the form

$$y^{5/2} = 1 + \frac{5}{2}\frac{\tau a_{max}}{\alpha R_0^2}[t - \tau(1 - e^{-t/\tau})]. \tag{1.8}$$

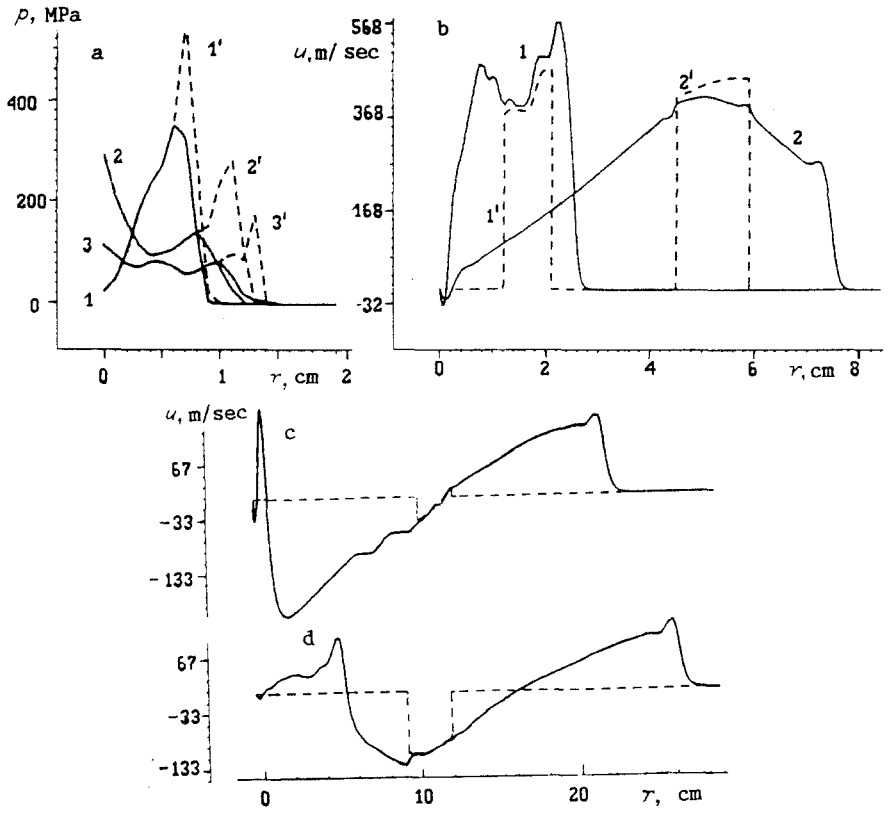

Fig. 14

Calculations using (1.6) and (1.8) for $k_0 = 10^{-10}$, $R_0 = 1$ μm, and $\tau = 10$ μsec show that at time $t = \tau$ the amplitude of the discharge wave in a cavitating liquid has decreased by a factor of 20e (in a one-phase medium the decrease is only by a factor of e). For $t \ll \tau$ the time dependence of the stress behind the rarefaction wave front is quite accurately determined by the equation

$$p \simeq -\rho_0 \left(a_{\max}^2 R_0^3 / 3k_0\right)^{2/5} t^{-2/5}. \tag{1.9}$$

This model can also be used to estimate the effect of the slope of the front on the limiting tensile stress p_{max} in a cavitating liquid. It is sufficient to consider only a part of the front and to approximate a(t) as a linear function of time: $a(t) = a_{max} t/\tau$, where $1/\tau$ determines the slope of the front. At $t = \tau$ the wave amplitude reaches a maximum and is determined by (1.9) with t replaced by τ. Assuming $k_0 = 10^{-11}$ and $R_0 = 0.5$ μm [6], and $\tau = 1$ μsec, $a_{max} = 3.28 \cdot 10^7$, we obtain $p_{max} \simeq -3$ MPa, instead of the expected value of 30 MPa. The calculations of [6] give a quantity of the same order, which shows the reliability of (1.9) in estimating both the relaxation time and the limiting tensile stress.

The complete system of equations (1.3), without any assumptions (such as on the state of the gas) and with heat transfer taken into account in the calculation of the pressure inside a bubble, was applied to the problem of a shock rarefaction tube. This is the analog of the classical shock tube where the liquid is contained in the high-pressure chamber and also the breakup of an arbitrary discontinuity with essentially unsteady and nonlinear conditions. Instead of assuming adiabatic conditions in the Rayleigh equation of (1.3), the gas pressure p_g was calculated from the equation

$$dp_g/dt = 3(\gamma - 1) q/4\pi R^3 - 3\gamma p_g (dR/dt)/R,$$

where the rate of heat transfer and the temperature are given by

$$q = 4\pi R^2 \lambda_g \mathrm{Nu}(T_0 - T)/2R, \quad T = p_g/(\gamma - 1) c_v \rho_g = T_0 (R/R_0)^3 p_g/p_{g0},$$
$$\mathrm{Nu} = \sqrt{\mathrm{Pe}} \text{ for } \mathrm{Pe} > 100, \quad \mathrm{Nu} = 10 \text{ for } \mathrm{Pe} < 100,$$
$$\mathrm{Pe} = 12(\gamma - 1) T_0 R |S|/\nu |T_0 - T_g|.$$

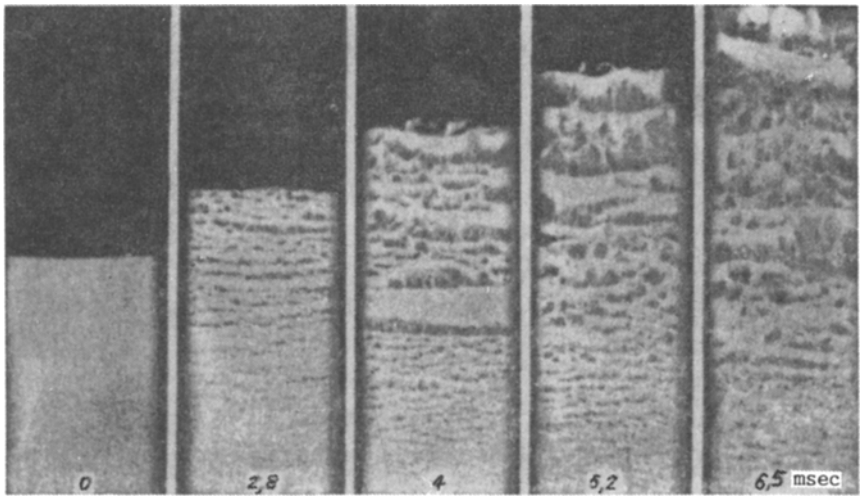

Fig. 15

The dynamical behavior of the rarefaction wave structure in a cavitating liquid was calculated for the following parameters: $\nu = 0.01$ cm^2/sec, $c_v = 0.718 \cdot 10^7$ cm^2/(sec^2·deg), $\lambda_g = 2470$ g·cm/(sec^3·deg), $k_0 = 10^{-4}$, $R_0 = 50$ μm [15].

Figure 7 shows the pressure distribution in the liquid at times t = 20 and 40 μsec (a) and 440 μsec (b). It is evident that the wave field splits up into two characteristic parts: a precursor forming a centered rarefaction wave and propagating with the "frozen" speed of sound of the unperturbed liquid, and the main disturbance in the form of a wave with an oscillating front and propagating with the equilibrium speed of sound of the two-phase bubbly medium. We note the analogy with the separation of shock waves in bubbly media into a precursor and a wave packet observed by the author in [16].

2. Transition to the Fragmentation Stage. Methods of Measurement. As noted above, for sufficiently intense rarefaction waves bubble cavitation is characterized by unbounded growth of nuclei from the entire theoretically possible size spectrum. Because the tensile stress relaxation time in the cavitation zone is small compared with the typical time required for buildup of the zone to volume concentrations of several dozen percent, the idea of a two-phase model with instantaneous relaxation has been proposed [17]. In this model the medium in the region behind the front of the rarefaction wave is characterized only by its inertial properties. The restrictions on the volume concentration are obviously removed in this approach and the zone can build up until the formation of a foamy structure.

Unfortunately our current understanding is incomplete of the essentially nonlinear processes of unbounded growth of bubbles in cavitation clusters, their hydrodynamic interactions in close-packed structures with volume concentrations of 0.5-0.75, and the transition through the foamy structure to the breakaway of sheets and the formation of the droplet phase. Therefore new experimental information and methods to determine the features of the process are of fundamental importance. We note that in solid-state mechanics two types of breakdown under pulse loading are usually considered: plastic and frangible breakdown. In the latter case the formation of discontinuities in the form of surfaces on which critical stresses arise is typical. Study of the flow structure of a cavitating liquid produced by an underwater explosion near the free surface shows that the breakdown of the liquid in intense discharge waves occurs by both mechanisms and cavitating sheets are observed [18] (Fig. 8). A cavitating liquid therefore displays a frangible property which is not chracteristic of an ideal liquid. The nature of this effect is still to be explained, as is the answer to the question of where in a large mass of cavitating liquid sheets are formed. The prerequisite to their formation is possibly built into the wave field from the very beginning.

We discuss a number of methods which more or less determine the basic elements of the process. The experiments of [17] with an exploding wire show in the case of axial loading of a cylindrical sample of liquid that the flow splits up into two zones: cavitating external and internal zones in the form of a liquid ring bordering a cavity containing the explosion

products. As the process develops the outer cavitation layer should break up into fragments (the medium is no longer continuous) and therefore a detector measuring dynamical head near the free surface should show a smooth transition from one state to the other. Figure 9a, in the form of three-dimensional diagrams of the pressure as a function of time and the distance δ to the free surface, shows the "two-pulse" structure of the stopping pressure. It is evident that the pulse corresponding to the flow of the cavitating liquid decreases sharply with increasing distance from the free surface. It practically disappears after 150-200 μsec because of the formation of a foamy structure as an intermediate step in the breakdown process. The second pulse corresponds to the layer of continuous liquid which becomes unstable and breaks up much later. The experiment shows that in reversible cavitation breakdown does not occur and the two pressure "waves" join together after a certain time.

The inversion can be detected more exactly by measuring the electric potential in the medium. It is well known that a potential difference occurs in a dispersed system when there is relative motion between the phases. The potential difference is in the direction of the relative velocity. The cause is the presence of an electric double layer on the boundary between the phases and flow-induced separation of ions adsorbed on the surfaces of bubbles or drops. The sign of the ions will depend on the particular two-phase structure. Therefore by measuring the instant when the potential changes sign, one can determine when inversion of the two-phase state has occurred. Measurements of this kind were carried out in [19] using a setup similar to [17]. They show that after approximately 500-600 μsec the inversion process is completed (Fig. 9b, where 1 is the cavitating liquid, 2 is the gas–droplet system, and the diagram is qualitative).

The opacity of the fully developed cavitation zone and the screening of its internal structure by a layer of bubbles on the wall of the shock tube makes the use of the standard high-speed optical motion pictures unsuitable. The use of x-ray pulses is much more promising [20].

The later optically opaque stage of the cavitation process in intense rarefaction waves was studied using three x-ray devices in a two-diaphragm hydrodynamic shock tube consisting of three sections: a high-pressure chamber, an evacuated acceleration channel (with the driving piston and two separating diaphragms on the ends), and the working section made of duralumin and containing the liquid under study. The lower diaphragm was ruptured by an electromagnetic system with a needle and the velocity of the piston against the upper diaphragm separating the channel from the liquid was measured with fiber-optic detectors. The entire system was synchronized: the three x-ray devices were started with different a priori time lags, thereby producing high-speed x-ray photographs. The average radiated energy was about 70 keV and the duration of a single burst was 80 nsec. A shock wave produced in the liquid sample was a result of impact of the piston. Its positive phase lasted several tens of microseconds and the amplitude varied between 20 and 30 MPa. Reflection of the shock wave from the free surface of the liquid produced strong cavitation, as shown by the x-ray photographs in Fig. 10 for different times from zero to 1 msec (the interval between frames is 200 μsec). We see that after 600 μsec the cavitation bubbles reach close packing with prominent vapor-gas cells.

Computer analysis of the images on the x-ray negatives was necessary in order to be able to freely analyze the dynamics of the process without interference by the detectors. The result is a computer-generated version of the experimental data which can easily be analyzed, giving a unique opportunity to reproduce the dynamics of the cavitation zone structure in an arbitrary cross section (the lower limit of resolution in the concentration was about 2%). Figure 11 shows a typical computer version of a stage of cavitation and the cross-sectional average local density distribution along a line parallel to the symmetry axis and separated from it by a distance of R/2. The volume concentration k of the vapor-gas phase along the cross section varied from zero (homogeneous liquid) up to values typical of a system with close packing of bubbles ($k \approx 75\%$).

The experiments show that before the process reaches the fragmentation stage, the zone of strong cavitation can be defined as the zone with close-packed bubbles where a chain of touching bubbles can fill the volume of the mixture by displacement by the bubble radius or by parallel transport. Assuming that the bubbles maintain their spherical shape and that the initial number of nuclei is of order 10^6 cm^{-3}, it is not difficult to show that the size of

the liquid fractions in the spaces between the touching bubbles in such structures varies between 7 and 25 μm, depending on the packing configuration. This estimate is for the central core, although starting from the packing configurations it should have several thin tails which can contribute micron-sized particles to the spectrum of the droplet structure of the nascent inversion two-phase medium during dispersion and breakdown.

3. On a Physical Model of Breakdown. The basic features of the breakdown process of a finite volume of liquid with a free surface produced by explosive loading (called cavitation breakdown [4]) can be described as follows. The reflection of the strong shock wave from the free surface leads to the formation of a discharge wave and behind its front strong bubble cavitation develops on microinhomogeneities acting as nuclei; these are always present in real liquids.

Unbounded growth of cavitation bubbles leads to the formation of the foamy structure in the bubbling liquid. The latter is finally transformed into the gas–droplet structure during inertial expansion, which, as noted above, starts because of tensile-stress relaxation. The duration of each phase of breakdown can be different in each case and depends strongly on the loading dynamics. However, the typical time scales of the process are determined from the experimental and numerical studies mentioned above: tensile-stress relaxation is of the order of microseconds, dense cavitation clusters develop over tens of microseconds, the foamy structure forms over hundreds of microseconds, and its breakup into liquid (possibly cavitating) fragments occurs over roughly a millisecond. Experimental and numerical studies of the final stage of the process are discussed below.

Since details of the transition from the foamy structure to the droplet structure are still unknown, we will assume that fragmentation occurs instantaneously when the cavitation zone structure reaches close packing. We then assume that the close packing of bubbles is instantaneously transformed into close-packed noncoagulating spherical elastic liquid droplets. The size spectrum of the droplets was estimated at the end of Sec. 2. This model can be called the sandy model since this structure of the medium is characterized only by elastic interactions between particles.

The obvious next step is the experimental comparison of the details of explosive breakdown of a continuous liquid and a sandy shell with all of the correct geometrical parameters of the charge–shell system.

High-speed motion pictures of the dispersion of both types of cylindrical shells under axial loading showed basically the identical structure of the resulting two-phase motion. Figure 12 shows a series of frames of the dispersing liquid and sandy cloud for two relative thicknesses of the systems: $R = (5-4)R_3$ (a) and $R = 10R_3$ (b). Note that the streamer structures of the gas–droplet and sandy flows occurring at the same time (and typical for thin shells) are identical. Note also the preservation of the cylindrical shape at large calibers.

To study the fine structure of the flow during the formation of a sandy cloud a special device was developed to measure the dynamics of the particle distribution at an arbitrary local point in the flow. It is a disk with a flat rim about 2 cm in height and radius of about 15 cm mounted on a motor shaft and capable of rotating with a linear velocity up to 150 m/sec. A strip was attached to the outer perimeter of the disk and pointing outward. The entire device was mounted inside a hermetically sealed housing with a small 2 × 2 cm window opposite to the strip and a ventilator. The trap was placed at a given distance from the charge–shell assembly and was brought to the required velocity in order to eliminate the possibility of repeated superposition of the flow. The required velocity was determined from the duration of the flow by analyzing evolution of the process in the neighborhood of the given point. Because the window in the trap was always open, it was not necessary to synchronize the startup of the trap with the process. Part of the flow entered the trap in the explosion and tiny particles were caught on the rotating strip. The time variation of the concentration of particles at the given point was thereby measured.

Figure 13 shows two scans of the structure of the sandy flow at distances of 0.6 (a) and 1 m (b). It is interesting to note that the flow is characterized by stratification of particles according to size. At 0.6 m the smaller particles are in the tail of the flow, while at 1 m the trap picks up only the large particles. The sandy cloud is therefore

strongly stratified: the small particles occupy the central zone and the large particles are distributed at the periphery.

This model, with its instantaneous transformation of the foamy structure into the droplet structure, was analyzed numerically [21]. A spherical charge of explosives with density ρ_0 and radius r_1 is surrounded by a two-phase shell of outer radius r_2 of liquid particles and air with a volume concentration of the dispersed phase of 74%, corresponding to close packing of spheres. Detonation of the charge was modeled as an instantaneous explosion at constant volume. The pressure of the detonation products was taken to be an average value and the density was ρ_0. The spherically symmetric motion of the two-phase mixture can be described by the following equations written separately for each component:

$$\rho_{1t} + r^{-2}(r^2\rho_1 u_1)_r = 0,$$
$$\rho_{2t} + r^{-2}(r^2\rho_2 u_2)_r = 0,$$
$$(\rho_1 u_1)_t + r^{-2}(r^2\rho_1 u_1^2)_r + \alpha_1 p_{2r} + [\alpha_1(p_1 - p_2)]_r = -f,$$
$$(\rho_2 u_2)_t + r^{-2}(r^2\rho_2 u_2)_r + \alpha_2 p_{2r} = f,$$
$$(\rho_2 e_2)_t + r^{-2}(r^2\rho_2 e_2 u_2)_r = \alpha_2 p_2(\rho_{2t}^0 + u_2\rho_{2r}^0)/\rho_2^0,$$
$$(\rho_1 E_1 + \rho_2 E_2)_t + r^{-2}[r^2(\rho_1 u_1 E_1 + \rho_2 u_2 E_2) + r^2(\alpha_1 u_1 p_1 + \alpha_2 u_2 p_2)]_r = 0.$$

Here $\rho_i = \rho_i{}^0\alpha_i$ $(i = 1, 2)$; $\alpha_1 + \alpha_2 = 1$; $f = 0.75\alpha_2\rho_1^0 C_d|u_1 - u_2|(u_1 - u_2)/d$; subscripts 1 and 2 refer to the gas and dispersed phases, d is the particle diameter, ρ_i, $\rho_i{}^0$, α_i u_i, p_i, E_i, e_i are the average and true densities, the volume concentration, the velocity, the pressure, and the total and internal energies of the i-th phase. The expressions for the drag coefficients were taken from [21]. The Tate equation of state was assumed for the dispersed phase. The system of equations was closed by the assumption of simultaneous deformation of the phases: when $\alpha_2 > 0.74$ the particles are assumed to deform such that they are stacked at the corners of right tetrahedrons and the surface of contact between two particles is a plane, but otherwise the particles preserve their spherical shape.

The large-particle method was used for the numerical calculations. In this method the velocity distributions of the phases are assumed to be far from equilibrium. Therefore for stability the right-hand sides of the momentum conservation equations were approximated by choosing one factor from the lower (in time) layer of the difference grid and another factor from the upper layer. The explosive was assumed to be hexogen with density $\rho_0 = 1.65$ g/cm^3 and caloricity 1.32 kcal/g. The other initial parameters of the problem were $r_1 = 0.3$ cm, $r_2 = 1.5$ cm, $e_1 = 5526$ J/g, $\rho_1 = 1.65$ g/cm^3, $\alpha_2 = 0.74$, $\rho_2{}^0 = 1$ g/cm^3, $u_2 = 0$, $e_2 = 0$. The medium external to the droplet shell was air with initial parameters $\rho_1 = 0.001$ g/cm^3, $u_1 = 0$, $e_1 = 250$ J/g.

The calculations were done for three species of liquid particles d = 1, 6, and 60 μm. Three stages of the process can be identified from the numerical results. The first stage is associated with the breakup of the discontinuity on the inner boundary of the two-phase region, which leads to a rarefaction wave in the detonation products and a shock wave in the gas and dispersed phase (dashed lines in Fig. 14a). The shock wave in the gas lags somewhat behind the shock wave in the liquid particles and its amplitude is much smaller (lines 1, 1'-3, 3' correspond to times of 3, 6, and 9 μsec in Fig. 14a). The shock wave compresses the dispersed phase and it acquires a velocity which is large compared to the gas velocity: the boundary of the detonation products does not keep up with the inner edge of the dispersed layer. After reaching the outer boundary a diverging shock wave is produced in the air while a rarefaction wave propagates through the particles. Together with divergent effects, the rarefaction wave leads to a rapid drop in tensile stress in the particles and their density drops below the close-packed value after 20 μsec (the particles separate and the shell becomes transparent).

In the second stage kinetic energy is transferred to the dispersed phase. This stage effectively ends after 60-70 μsec, when the pressure in the detonation products drops to atmospheric pressure and the particles begin to decelerate (Fig. 14b shows the mass velocity distribution for t = 20 and 100 μsec, lines 1, 1' and 2, 2'). In the third stage the rarefaction wave accumulates toward the center and there is a strong return flow of the gas (Fig. 14c, t = 350 μsec), which brakes and then carries off small particles toward the center (Fig. 14d,

t = 500 μsec), thus producing the size stratification observed experimentally. This effect also produces a sharp (by about a factor of 40) increase in the thickness of the two-phase layer as the inner and outer radii reach their asymptotic values. Wave processes in the gas phase have a strong effect on the dynamics of the inner boundary of the layer, which oscillates with a frequency characteristic of these processes.

The sandy model of one of the stages of the breakdown of a liquid under explosive loading may find an interesting extension in the framework of the experimental studies of the flow structure of a dusty layer in a rarefaction wave carried out by Sturtevant at California Institute of Technology [22].

In the experiments of [22] a 60 cm layer of glass balls of diameter 125 μm was packed on the bottom of a cylindrical chamber filled with air at atmospheric pressure and separated from a high-pressure chamber (0.31 MPa) by a diaphragm. After rupture of the diaphragm a rarefaction wave propagated in the air gap, reached the layer boundary, reflected from it, and was partially refracted inside the layer. The experiments show that the refracted wave induced a rapid expansion of gas into the pores between the particles. Horizontal sheet discontinuites of the type seen in liquids (Fig. 15 of [22]) were observed, which then transformed into a system of cavities forming a honeycomb structure (compare Fig. 10). According to the experimental data of [22] the thickness of the separated sheets in the dusty layer was several times the particle diameter. In the upper part of the layer the particles obtained an average acceleration of about 275 g in the first 5 msec and reached velocities of about 15 m/sec. We note that the density of particles in the dusty layer was about $5 \cdot 10^5$ cm^{-3} and corresponds to the density of cavitation nuclei in real liquids, while the layer itself models the state of a cavitating liquid when the bubble zone reaches the close-packed density.

The analysis discussed here of certain essentially nonlinear effects determining the behavior of real liquids under explosive loads shows that, in spite of the complexity of the problem, it is possible to construct adequate mathematical models describing wave processes in cavitating and disintegrating liquids. The experimental methods discussed here may provide answers to a number of fundamental questions on the mechanics of liquid breakdown.

Unsolved problems include the mechanism of "frangible" breakdown of the foamy structure and the foam–droplet transition, the development of methods capable of resolving the entire possible spectrum of nuclei, the stability of combination structures of the type gas nucleus–solid particle, the metastable state of a liquid in the deep negative phase, and the kinetics of the formation of vapor centers on the front of an intense rarefaction wave.

LITERATURE CITED

1. D. H. Trevena, Cavitation and Tension in Liquids, A. Hilger, Bristol (1987).
2. D. A. Wilson, J. W. Hoyt, and J. W. McKune, "Measurement of tensile strength of a liquid by explosion technique," Nature, 253, No. 5494 (1975).
3. G. A. Carlson and K. W. Henry, "Technique for studying tension failure in application to glycerol," J. Appl. Phys., 42, No. 5 (1973).
4. V. K. Kedrinskii, "Surface effects in underwater explosions (review)," Prikl. Mekh. Tekh. Fiz., No. 4 (1978).
5. R. H. Cole, Underwater Explosions, Princeton University Press, Princeton, NJ (1948).
6. V. K. Kedrinskii, "Negative pressure profile in cavitation zone at underwater explosion near the free surface," Acta Astronautica, 3, No. 7-8 (1976).
7. A. S. Besov, V. K. Kedrinskii, and E. I. Pal'chikov, "Study of the initial stage of cavitation, using optical diffraction," Pis'ma Zh. Tekh. Fiz., 10, No. 4 (1984).
8. F. G. Hammitt, A. Koller, O. Ahmed, et al., "Cavitation threshold and superheat in various fluids," Proc. Conf. on Cavitation, Edinburg, 1974, Mech. Eng. Publ., London (1976).
9. V. K. Kedrinskii, "Peculiarities of bubble spectrum behavior in cavitation zone and its effect on wave field parameters," Ultrasonics Intern. 85, London, Gilford (1985).
10. V. K. Kedrinskii, "On the relaxation of tensile stresses in cavitating liquid," 13th Int. Congress on Acoustics, Beograd, 1989, Dragan Srnic Press, Sabac (1989).
11. M. G. Sirotyuk, "Experimental study of ultrasonic cavitation," Strong Ultrasound Fields [in Russian], Part 5, Nauka, Moscow (1968).

12. V. K. Kedrinskii, "On multiplication mechanism of cavitation nuclei," 12th Int. Congress on Acoustics, Toronto (1986).
13. V. K. Kedrinskii, V. V. Kovalev, and S. I. Plaksin, "On a model of bubble cavitation in real liquids," Prikl. Mekh. Tekh. Fiz., No. 5 (1986).
14. I. Hansson, V. Kedrinskii, and K. Morch, "On the dynamics of cavity clusters," J. Phys. D, 15, (1982).
15. V. Kedrinskii and S. Plaksin, "Rarefaction wave structure in cavitating liquid," Problems in Nonlinear Acoustics: Trans. Symp. IUPAP-IUTAM on Nonlinear Acoustics, Novosibirsk (1987), Ch. 1.
16. V. K. Kedrinskii, "Propagation of disturbances in a liquid containing gas bubbles," Prikl. Mekh. Tekh. Fiz., No. 4 (1968).
17. N. N. Chernobaev, "Modelling of shock-wave loading of liquid volumes," Adiabatic Waves in Liquid Vapor Systems, Proc. IUTAM Symp., Gottingen, 1989, Springer, Berlin (1989).
18. V. K. Kedrinskii, Experimental research and hydrodynamical models of a 'sultan'," Arch. Mech., 26, No. 3 (1974).
19. S. V. Stebnovskii, "On the mechanism of pulse breakdown of a liquid volume," Prikl. Mekh. Tekh. Fiz., No. 2 (1989).
20. A. R. Berngardt, E. T. Bichenkov, V. K. Kedrinskii, and E. I. Pal'chikov, "Optic and x-ray investigation of water fracture in a rarefaction wave at a later stage," in: Optical Methods in Dynamics of Fluids and Solids, Proc. IUTAM Symp., Prague, 1984, Spinger, Berlin (1985).
21. I. G. Gets and V. K. Kedrinskii, "Dynamics of the bubble breakdown of a finite volume of a two-phase mixture," Prikl. Mekh. Tekh. Fiz., No. 2, (1989).
22. A. V. Anilkumar, "Experimental studies of high-speed dense dusty gases," Thesis, Pasadena (1989).